CHEMISTRY OF MATERIALS

pubs.acs.org/cm

Article

# Two-Dimensional Copper Iodide-Based Inorganic–Organic Hybrid Semiconductors: Synthesis, Structures, and Optical and Transport Properties

Wooseok Ki,[#] Xiuze Hei,[#] Hee Taek Yi, Wei Liu, Simon J. Teat, Mengjun Li, Yang Fang, Vitaly Podzorov, Eric Garfunkel, and Jing Li*

Cite This: *Chem. Mater.* 2021, 33, 5317–5325

Read Online

ACCESS | Metrics & More | Article Recommendations | Supporting Information

**ABSTRACT:** A group of copper iodide-based hybrid semiconductors with the general formula of 2D-CuI$(L)_{0.5}$ ($L$ = organic ligands) are synthesized and structurally characterized. All compounds are two-dimensional (2D) networks made of one-dimensional (1D) copper iodide staircase chains that are interconnected by bidentate nitrogen-containing ligands. Results from optical absorption and emission experiments and density functional theory (DFT) calculations reveal that their photoluminescence (PL) can be systematically tuned by adjusting the lowest unoccupied molecular orbital (LUMO) energies of the organic ligands. Charge carrier transport measurements were carried out for the first time on single crystals of selected 2D-CuI$(L)_{0.5}$ structures, and the results show that they possess p-type conductivity with a Hall mobility of ~1 cm$^2$ V$^{-1}$ s$^{-1}$ for 2D-CuI$(pm)_{0.5}$ and 0.13 cm$^2$ V$^{-1}$ s$^{-1}$ for 2D-CuI$(pz)_{0.5}$, respectively. These values are comparable to or higher than the mobilities of typical highly luminescent organic semiconductors. This work suggests that robust, high-dimensional copper iodide hybrid semiconductors are promising candidates to be considered as a new type of emissive layer for light-emitting diode (LED) devices.

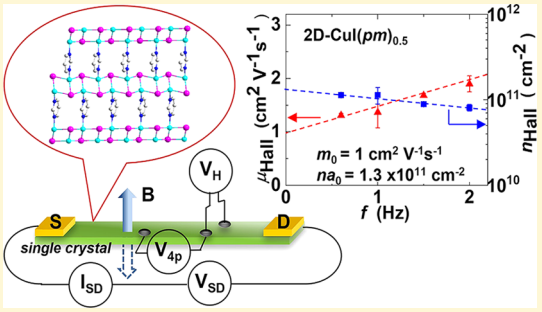


## INTRODUCTION

While high-performance photoluminescent (PL) materials are very important for general lighting applications, there has also been an increasing demand for highly efficient electroluminescent (EL) materials for use in full-color, light-weight, and flexible displays as well as various light-emitting diode (LED) devices.[1,2] Either poor charge transport or low luminescence efficiency remain to be the two main challenges for organic semiconductors currently used in organic light-emitting diodes (OLEDs). For example, strongly emissive organic materials such as tris(8-hydroxy quinoline) aluminum ($Alq_3$) or phenylenevinylene-based polymers show poor charge transport with low carrier mobilities ($10^{-6}$–$10^{-5}$ cm$^2$ V$^{-1}$ s$^{-1}$).[3,4] On the other hand, high-mobility (>1 cm$^2$ V$^{-1}$ s$^{-1}$) organic semiconductors typically exhibit very low luminescence quantum efficiency because of their aggregation-induced quenching.[5−7] Conversion of short-lived singlet excitons to long-lived triplets via the intersystem crossing in rare-earth element (REE) containing organic molecules, such as Ir or Eu-based complexes, has proven to be an effective approach for improving the device efficiency, but these elements are very costly.[8,9] In addition, thermal evaporation under high vacuum is typically used for the fabrication of small-molecule-based active layers in OLEDs, which suffers from low throughput and high cost.[10,11] Therefore, developing highly luminescent, low-cost, solution-processable semiconductors with tunable band gaps and relatively high charge carrier mobilities represents a major leap forward in the future development of light-emitting diode (LED) technologies.

Copper iodide-based crystalline inorganic–organic hybrid materials have attracted great attention in recent years due to their structural diversity and unique optical properties, which demonstrate strong potential for general lighting-related applications.[12−21] Several types of structures with different inorganic building motifs have been developed, and intensive studies have been carried out to improve their optical properties and chemical/thermal stabilities.[22,23] However, investigation of their electrical properties as EL materials remains underexplored. Among numerous types of structures, those that are built of one-dimensional (1D) CuI chains are of particular interest, as the infinite chains of the inorganic motif may act as a highly efficient pathway for charge transport, thereby generating high carrier mobility required for good EL

Received: April 24, 2021
Revised: June 17, 2021
Published: June 30, 2021

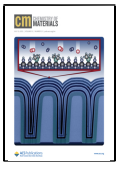

Downloaded via RUTGERS UNIV on July 13, 2022 at 02:09:30 (UTC).
See https://pubs.acs.org/sharingguidelines for options on how to legitimately share published articles.

ACS Publications

© 2021 American Chemical Society

materials, and the organic ligands in these structures would be largely responsible for their optical tunability.[24−28]

To test out the abovementioned hypothesis, we synthesized a series of 2D-CuI$(L)_{0.5}$ compounds containing infinite 1D chains of copper iodide. Bidentate ligands, including bipyridine, pyrazine, pyrimidine, imidazole, and their derivatives, were used for the construction of these two-dimensional (2D) network structures with the neighboring chains interconnected by the ligands. All structures have the formula 2D-CuI$(L)_{0.5}$, where $L$ is a bidentate ligand. Large millimeter-sized single crystals of 2D-CuI$(pm)_{0.5}$ and 2D-CuI$(pz)_{0.5}$ were obtained by a slow-diffusion growth method and were used for electrical property studies. Results from Hall-effect measurements indicate that they have high charge carrier mobilities (up to ∼1 $cm^2 V^{-1} s^{-1}$), which are significantly higher than those of typical highly luminescent organic semiconductors.

## EXPERIMENTAL SECTION

**Materials.** CuI (98%, Alfa Aesar), acetonitrile (ACN, >99%, Alfa Aesar), pyrimidine (*pm*, 98%, Alfa Aesar), pyrazine (*pz*, 98%, Alfa Aesar), 1,2-bis(4-pyridyl)ethane (*bpe*, 99%, Sigma-Aldrich), 1,2-bis(4-pyridyl)ethylene (*bpee*, 97%, Sigma-Aldrich), 4,4′-bipyridyl (4,4′-*bpy*, >98.0%, TCI), 1,4-bis(bromomethyl)benzene (97%, Alfa Aesar), benzimidazole (99%, Alfa Aesar), dimethyl sulfoxide (DMSO, >99%, Alfa Aesar), NaOH (98%, Alfa Aesar), sodium salicylate (99%, Merck), YAG:$Ce^{3+}$ type 9800 (Global Tungsten & Powders Corp), and potassium iodide (KI; 99%, Alfa Aesar) were used in the experiment. All chemicals were used as received without further purifications.

**Synthesis of 1,4-bis((1*H*-benzo[*d*]imidazol-1-yl)methyl)-benzene (*bbimb*).** A total of 1.2 g (30 mmol) of NaOH was added to a solution of 1.18 g (10 mmol) of benzimidazole in 20 mL of dimethyl sulfoxide (DMSO). The mixture was stirred at 70 °C for 2 h, followed by injection of 540 μL (4 mmol) of 1,4-bis(bromomethyl)-benzene into the solution. The reaction mixture was heated at 100 °C overnight. After cooling to room temperature, the solution was then poured into 150 mL of cold water for 3 h. The solution was extracted with methylene chloride three times, and the combined extract was concentrated in vacuum to a white solid. The pure product of *bbimb* in a high yield (80%) was obtained after recrystallization with an acetone/hexane (v/v = 1:1) solution.

*General Synthesis Procedures of Compounds **1**−**6**.* Single crystals of 2D-CuI$(pm)_{0.5}$ (**1**), 2D-CuI$(pz)_{0.5}$ (**2**), 2D-CuI$(4,4'\text{-}bpy)_{0.5}$ (**3**), 2D-CuI$(bpe)_{0.5}$ (**4**), 2D-CuI$(bpee)_{0.5}$ (**5**), and 2D-CuI$(bbimb)_{0.5}$ (**6**) were acquired by a slow-diffusion method.[29] The reactions were conducted in glass vials at room temperature. The bottom, middle, and top layers were a CuI/KI-saturated aqueous solution, acetonitrile, and a ligand in ethanol, respectively. The crystals formed in the middle layer over 3−5 days at room temperature. Pure phase powder samples were obtained by direct mixing of CuI (0.019 g, 0.1 mmol) in a saturated KI solution with a ligand (0.1 mmol) in ethanol. The ligand solution was added dropwise to prevent the formation of different phases. The pure phase powder generally formed immediately after stirring. Mild heating at 60 °C overnight may be helpful for obtaining samples of higher crystallinity. Larger single crystal growth for electrical measurements was obtained by a similar method under optimized conditions.

*Synthesis of Compound **1**.* CuI (0.19 g, 1 mmol) was first dissolved in a KI-saturated solution (2 mL) in a reaction vial. Acetonitrile (2 mL) was added as another layer, and then *pm* (1 mmol) in methanol (2 mL) was slowly added to the vial. The reaction mixture was kept undisturbed at room temperature, and plate-shaped single crystals were formed in 3 days and collected by filtration. The yield was 45%. Millimeter-sized single crystals of 2D-CuI$(pm)_{0.5}$ were grown by a modified diffusion growth method. A solution of CuI (0.19 g, 1.0 mmol) in a saturated potassium iodide (KI) solution (2.0 mL) and a solution of 0.5 mmol *pm* in ethanol (2.0 mL) was separated by a layer of 2.0 mL of acetonitrile used as a middle layer. The solution was then placed in an oven at 60 °C for 1 day, which is necessary to grow large and thin plate crystals.

*Synthesis of Compound **2**.* Acetonitrile (2 mL) was added to a KI-saturated solution (2 mL) containing CuI (0.19 g, 1 mmol), and then *pz* (1 mmol) in methanol (2 mL) was slowly added. Plate-shaped single crystals were formed in 1 day and collected by filtration. The yield was 60%. The millimeter-sized single crystals were synthesized in the same way as compound **1**.

*Synthesis of Compound **3**.* CuI (0.19 g, 1 mmol) was first dissolved in a KI-saturated solution (2 mL) in a reaction vial. Acetonitrile (2 mL) was added as another layer, and then 4.4′-*bpy* (1 mmol) in methanol (2 mL) was slowly added to the vial. The reaction mixture was kept undisturbed at room temperature, and cube-shaped single crystals were formed in 3 days and collected by filtration. The yield was 45%.

*Synthesis of Compound **4**.* Acetonitrile (2 mL) was added in a KI-saturated solution (2 mL) containing CuI (0.19 g, 1 mmol), and then *bpe* (1 mmol) in methanol (2 mL) was slowly added. Needle-shaped single crystals were formed in 1 day and collected by filtration. The yield was 60%.

*Synthesis of Compound **5**.* CuI (0.19 g, 1 mmol) was first dissolved in a KI-saturated solution (2 mL) in a reaction vial. Acetonitrile (2 mL) was added, and then *bpee* (1 mmol) in methanol (2 mL) was slowly added to the vial. The reaction mixture was kept at 60 °C for 1 day, and the orange crystalline powder formed was collected by filtration. The yield was 75%.

*Synthesis of Compound **6**.* CuI (0.19 g, 1 mmol) was first dissolved in a KI-saturated solution (2 mL) in a reaction vial. Acetonitrile (2 mL) was added, and then *bbimb* (1 mmol) in methanol (2 mL) was slowly added to the vial. The reaction mixture was kept at 60 °C for 1 day, and the crystalline powder was collected by filtration. The yield was 55%.

**Single-Crystal X-ray Diffraction (SXRD) and Powder X-ray Diffraction (PXRD) Analysis.** Single-crystal diffraction data were collected using a D8 goniostat equipped with a Bruker PHOTON100 CMOS detector using synchrotron radiation at the Advanced Light Source (ALS), Lawrence Berkeley National Laboratory. The refinement method used was full-matrix least-squares on $F^2$. CCDC numbers are: 2005656 and 2077521. Powder X-ray diffraction (PXRD) analyses were carried out on a Rigaku Ultima-IV unit using Cu K$\alpha$ radiation ($\lambda$ = 1.5406 Å). The data were collected at room temperature in a 2$\theta$ range of 3−40° with a scan speed of 2°/min. The operating power was 40 kV/40 mA.

**Thermogravimetric Analysis (TGA).** Thermogravimetric analyses (TGA) were performed on powder samples using the TA Instrument Q5000IR thermal gravimetric analyzer with a nitrogen flow and a sample purge rate of 10 and 12 mL/min respectively. About 1−3 mg of samples was loaded onto a platinum sample pan and heated from room temperature to 450 °C at a rate of 10 °C/min under a nitrogen flow.

**Optical Measurements.** Optical absorption spectra were measured at room temperature on a Shimadzu UV-3600 UV/VIS/NIR spectrometer. The reflectance data were converted to the Kubelka−Munk function, $\alpha/S = (1 - R)^2/2R$ ($\alpha$ is the absorption coefficient, $S$ is the scattering coefficient, and $R$ is the reflectance), and used to estimate the band gap. The scattering coefficient ($S$) was treated as a constant, as the average particle size of the samples used in the measurements was significantly larger than 5 μm. Samples for optical reflectance measurements were prepared by evenly distributing ground powders between two quartz slides. Photoluminescence (PL) measurements were carried out on a Varian Cary Eclipse spectrophotometer at room temperature. Powder samples were evenly distributed and sandwiched between two glass slides (which do not have emission in the visible range) for all measurements. The internal quantum yield (IQY) of samples in the powder form was measured on a C9920-03 absolute quantum yield measurement system (Hamamatsu Photonics) with a 150 W xenon monochromatic light source and a 3.3 integrating sphere. Sodium salicylate and YAG:$Ce^{3+}$ were chosen as the standards with an IQY of 60 and 95% at 360 and 455 nm, respectively.[30,31] Their IQY values were measured to


https://doi.org/10.1021/acs.chemmater.1c01421
Chem. Mater. 2021, 33, 5317−5325

be 66 and 99%, respectively, which were used to calibrate the values obtained from other samples.

**Scanning Kelvin Probe Microscope (SKPM) Measurements.** These experiments were conducted on a Park Systems model NX-10 AFM with an EFM mode. The tip used was NSC14/CR-AU from MikroMasch. The energy resolution was ∼10 meV and the spatial resolution was ∼30 nm. Highly oriented pyrolytic graphite (HOPG) was used as a reference, and its surface potentials before and after measurements of the samples displayed a consistent value, confirming that the tip stays in the same condition when measuring the samples. An ultraviolet photoelectron spectroscopy (UPS) experiment was then performed on HOPG to obtain its absolute work function, which was estimated to be 5.5 eV. The potential difference between HOPG and the tip was around 8 mV. Considering the resolution of the Kelvin probe microscope (KPM), the intrinsic potential was calculated to be 5.50 V. The average potential differences of 2D-Cu($pm$)$_{0.5}$ and 2D-Cu($pz$)$_{0.5}$ were then measured to be −34 and −240 mV, respectively. As a result, the work functions of 2D-Cu($pm$)$_{0.5}$ and 2D-Cu($pz$)$_{0.5}$ were determined to be 5.46 and 5.26 eV, respectively.

**Hall-Effect Measurements.** Prior to the Hall-effect measurements, single crystals were sonicated in isopropyl alcohol for 5 s to clean the surface. Electrical contacts were painted on top of the crystals with an aqueous solution of colloidal graphite (Ted Pella) and contacted with 25 $\mu$m thick gold wires. Hall measurements were performed at room temperature in air. We used a DL1201 voltage preamplifier (DL Instruments) and a Stanford Research SR-830 lock-in amplifier for Hall voltage measurements, the Keithley current source K6221 for ISD excitation, and the Electrometer K6514 for four-probe voltage measurements. An ac magnetic field of a frequency 0.6−2 Hz with a root-mean-square magnitude of Brms = 0.23 T was generated by rotating an assembly of strong permanent Nd magnets fixed on an Al frame.

## RESULTS AND DISCUSSION

**Crystal Growth and Structures.** Various approaches have been developed to grow single crystals of copper halide-based hybrid structures. Among them, slow diffusion is one of the most efficient methods for obtaining high-quality crystals of chain-type structures. Because of the fast nucleation rate, these compounds generally precipitate out immediately after direct mixing of the copper iodide with the ligands at room temperature. To slow down the reaction and to promote the crystallization process, a third solvent, namely, acetonitrile, was used in our synthesis as a buffer layer and was placed between two solutions containing copper iodide (CuI/KI aqueous solution) and the ligand (methanol solution). With this approach, we obtained high-quality crystal samples of six compounds: 2D-CuI($pm$)$_{0.5}$ (**1**), 2D-CuI($pz$)$_{0.5}$ (**2**), 2D-CuI(4,4′-$bpy$)$_{0.5}$ (**3**), 2D-CuI($bpe$)$_{0.5}$ (**4**), 2D-CuI($bpee$)$_{0.5}$ (**5**), and 2D-CuI($bbimb$)$_{0.5}$ (**6**). Compounds **3** and **6** are new structures, and their crystallographic data are summarized in Table 1. Powder samples of these compounds could be obtained by directly mixing the ligands with a CuI/KI solution, and their phase purity has been confirmed by PXRD analysis (Figure S2). It is worth mentioning that the amount of ligands used has a notable influence on the final product. The targeted 2D-CuI($L$)$_{0.5}$ structures would form preferably under ligand-deficient conditions, so ligands must be added slowly into the CuI solution with a controlled amount to avoid the formation of other types of structures. Adding a ligand quickly or in excess amount might lead to the formation of $Cu_2I_2$ dimer-based structures.

All six structures are composed of staircase chains of 1D-CuI linked by bidentate ligands, giving rise to an overall 2D network (Figure S1). A typical structure is shown in Figure 1.

**Table 1. Summary of Crystal Data of New 2D-CuI(L)$_{0.5}$ Structures**

| compound | 2D-CuI($bpe$)$_{0.5}$ (**3**) | 2D-CuI($bbimb$)$_{0.5}$ (**6**) |
|---|---|---|
| crystal system | triclinic | monoclinic |
| empirical formula | $C_6H_6CuIN$ | $C_{11}H_9CuIN_2$ |
| FW | 282.56 | 359.64 |
| space group | $P\bar{1}$ | $P2_1/c$ |
| $a$ (Å) | 4.2051(4) | 4.4331(2) |
| $b$ (Å) | 9.0869(8) | 16.9180(6) |
| $c$ (Å) | 10.1661(8) | 13.7095(5) |
| $\alpha$ (deg) | 102.183(5) | 90 |
| $\beta$ (deg) | 95.680(6) | 97.495(2) |
| $\gamma$ (deg) | 97.483(6) | 90 |
| $V$ (Å$^3$) | 373.26(6) | 1019.42(7) |
| $Z$ | 2 | 4 |
| $T$ (K) | 298(2) | 100(2) |
| $\lambda$ (Å) | 0.7749 | 0.7749 |
| $R_1$ | 0.0319(1437) | 0.0172(3696) |
| w$R_2$ | 0.0718(1632) | 0.0425(3874) |

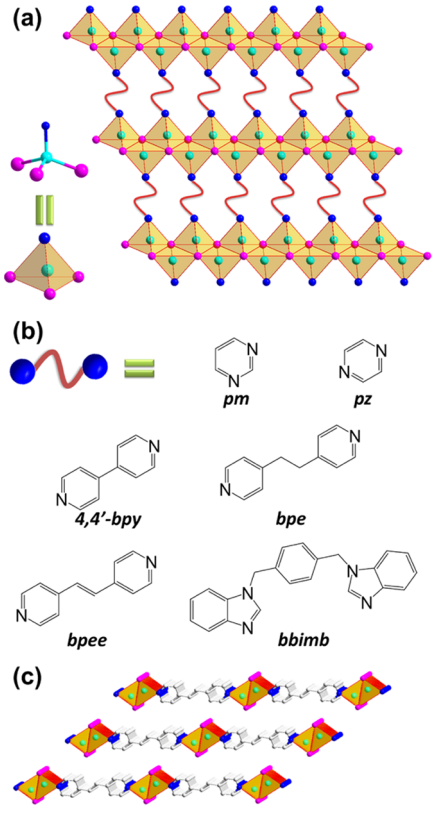


**Figure 1.** (a) Polyhedral representation of 2D-CuI($L$)$_{0.5}$. 1D-CuI chains are connected by bidentate ligands. (b) Bidentate ligands used in this work. (c) View of 2D-CuI($bpe$)$_{0.5}$, illustrating the staggered arrangement of adjacent sheets (Cu: cyan, I: pink, N: blue, and gray: C).

By varying the length of the bridging ligand, the separation between adjacent CuI chains can be easily controlled (Table 2), which is from 5.75 to 14.77 Å, measured as the distance between the two closest copper atoms from two adjacent chains. The distances between the adjacent sheets vary from 7.02 to 9.23 Å, and are also summarized in Table 2. It is worth noting that the distances between the adjacent ligands range from 3.40 to 3.77 Å, well within the length scale of $\pi-\pi$


https://doi.org/10.1021/acs.chemmater.1c01421
Chem. Mater. 2021, 33, 5317−5325

**Table 2. Interchain and Interlayer Distances in 2D-CuI($L$)$_{0.5}$**

| compound | interchain (Å) | interlayer (Å) | ligand $\pi-\pi$ distance (Å) |
|---|---|---|---|
| 2D-CuI($pm$)$_{0.5}$ | 5.75 | 7.02 | 3.66 |
| 2D-CuI($pz$)$_{0.5}$ | 6.86 | 6.25 | 3.56 |
| 2D-CuI(4,4′-$bpy$)$_{0.5}$ | 11.19 | 8.14 | 3.62 |
| 2D-CuI($bpe$)$_{0.5}$ | 13.45 | 8.31 | 3.77 |
| 2D-CuI($bpee$)$_{0.5}$ | 13.51 | 8.30 | 3.60 |
| 2D-CuI($bbimb$)$_{0.5}$ | 14.77 | 9.23 | 3.40 |

interactions. Such interactions may also contribute to mobility.[32]

**Optical Properties.** The optical absorption spectra of compounds **1**−**6** were recorded at room temperature and converted to the Kubelka−Munk function. The band gaps were estimated from their absorption edges. The values are 2.5, 2.25, 2.3, 3.1, 2.2, and 2.35 eV, respectively, for **1**−**6** (see Figure 2a and Table 3). This trend correlates well with that of the LUMO energies of the organic ligands in the structures (see Table S1). As shown in Figure 2b and Table 3, except compound **6**, other structures all emit in the visible-light region and their emission colors range from purple to red. Their emission profiles are all single-band type, with an average of full-width at half-maximum (FWHM) of ∼100 nm. The emission energies of these compounds are also in trend with their band gaps and the LUMO energies of the corresponding ligands. Their excitation spectra can be found in Figure S3.

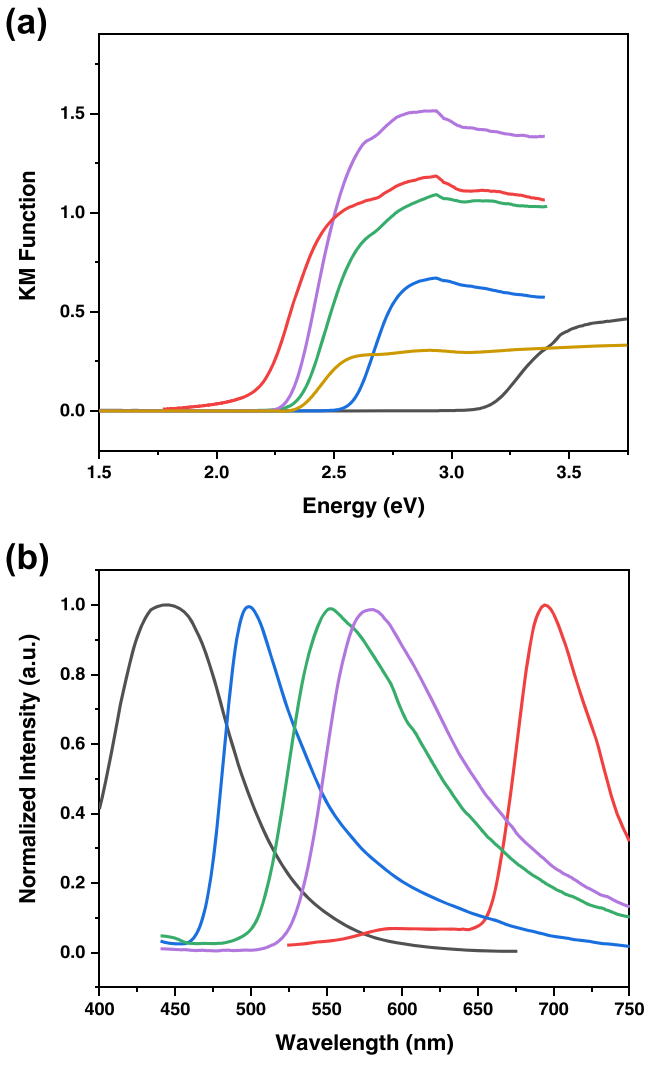


**Figure 2.** (a) Absorption spectra of **1** (blue), **2** (purple), **3** (green), **4** (black), **5** (red), and **6** (yellow). The steps near 3.4 eV in (a) were caused by the detector changing of the instrument. (b) Photoluminescence spectra of **1** (blue), **2** (purple), **3** (green), **4** (black), and **5** (red); $\lambda_{ex}$ = 360 nm.

**Thermal Stability Analysis.** The decomposition temperatures of compounds **1**−**6** were determined by the thermogravimetric (TG) analyses, and the results are listed in Table 3. Most of them are stable up to 250 °C, much more stable than those of 1D-CuI($L$) structures, which generally decompose around 100 °C (Figure 3a). Compound **3** was selected for a series of stability measurements, and the results show that it exhibits excellent thermal, chemical, and photo stabilities. After heating in an oven at 180 °C, soaking in water, placing under UV light for a week, the sample still maintains its structure and initial crystallinity based on the PXRD analysis (Figure 3b). The significantly enhanced stability of these structures is due to the formation of higher dimensionality as well as the use of ligands that form strong Cu−N bonds.[21,23]

**Electronic Structures.** To understand the electronic structures of these compounds, we performed density functional theory (DFT) calculations on selected structures. Generally, their band structures are generally dispersive, suggesting potentially good charge transport properties. The projected density of states (PDOS) analysis shows that for all compounds, the valance band maximum (VBM) is composed primarily of the atomic orbitals of an inorganic motif (i.e., Cu 3d and I 5p atomic orbitals), whereas the conduction band minimum (CBM) mainly consists of the atomic orbitals of organic ligands (i.e., C 2p and N 2p), similar to many reported CuX-based hybrid materials with a (M + X)LCT emission mechanism[13,17,19,24] (Figures 4 and S4−S8).

**Electrical and Transport Properties.** Growing crystals large enough for electrical property measurements has always been a challenging task. 2D-CuI($pm$)$_{0.5}$ and 2D-CuI($pz$)$_{0.5}$ were chosen for electrical and transport property studies as they emit at green ($\lambda_{em}$ = 500 nm) and yellow ($\lambda_{em}$ = 578 nm) wavelengths with relatively high quantum yields of 17.0 and 12.7% under 360 nm excitation, respectively (Table 3). Using a modified diffusion growth method, we were able to obtain both compounds with sufficiently large crystals. After a careful screening, two large plate-shaped and millimeter-sized high-quality single crystals of CuI($pm$)$_{0.5}$ and 2D-CuI($pz$)$_{0.5}$ (Figure 5) were selected for Hall mobility and carrier density measurements.

The knowledge of transport parameters, such as intrinsic carrier mobility, dark and photoconductivity, and carrier density, is essential for further development of CuI-based hybrid optoelectronic materials and devices. The intrinsic charge transport properties of 2D-CuI($pm$)$_{0.5}$ and 2D-CuI($pz$)$_{0.5}$ single crystals were investigated using the recently developed highly sensitive ac Hall-effect measurement technique.[33,34] This method allows for reliable measurements of the intrinsic Hall mobility and carrier density in highly resistive low-$\mu$ materials, such as organic semiconductors with carrier mobility as low as $\mu \sim 0.1$ cm$^2$ V$^{-1}$ s$^{-1}$. It is virtually impossible to resolve the Hall effect in such low-$\mu$ semiconductors using conventional dc Hall measurements even in very high magnetic fields (∼10 T). The novel method uses


https://doi.org/10.1021/acs.chemmater.1c01421
Chem. Mater. 2021, 33, 5317−5325

**Table 3. Estimated Band Gaps, Emission Energies, Colors, and Decomposition Temperatures ($\lambda_{ex}$ = 360 nm)**

| # | compound | BG (eV) | $\lambda_{em}$ (nm) | emission color | IQY (%) | crystal shape | crystal size(mm) | $T_D$ (°C) |
|---|---|---|---|---|---|---|---|---|
| 1 | 2D-CuI($pm$)$_{0.5}$ | 2.5 | 500 | green | 17.0 | plate | ~2 | 160 |
| 2 | 2D-CuI($pz$)$_{0.5}$ | 2.25 | 578 | yellow | 12.7 | plate | ~1 | 170 |
| 3 | 2D-CuI(4,4′-$bpy$)$_{0.5}$ | 2.3 | 556 | yellow | 2.5 | cubic | ~0.3 | 290 |
| 4 | 2D-CuI($bpe$)$_{0.5}$ | 3.1 | 443 | purple | 16.4 | needle | ~0.2 | 280 |
| 5 | 2D-CuI($bpee$)$_{0.5}$ | 2.2 | 695 | red | 1.0 | rod | ~2 | 300 |
| 6 | 2D-CuI($bbimb$)$_{0.5}$ | 2.35 | N/A | N/A | N/A | plate | ~0.1 | 310 |

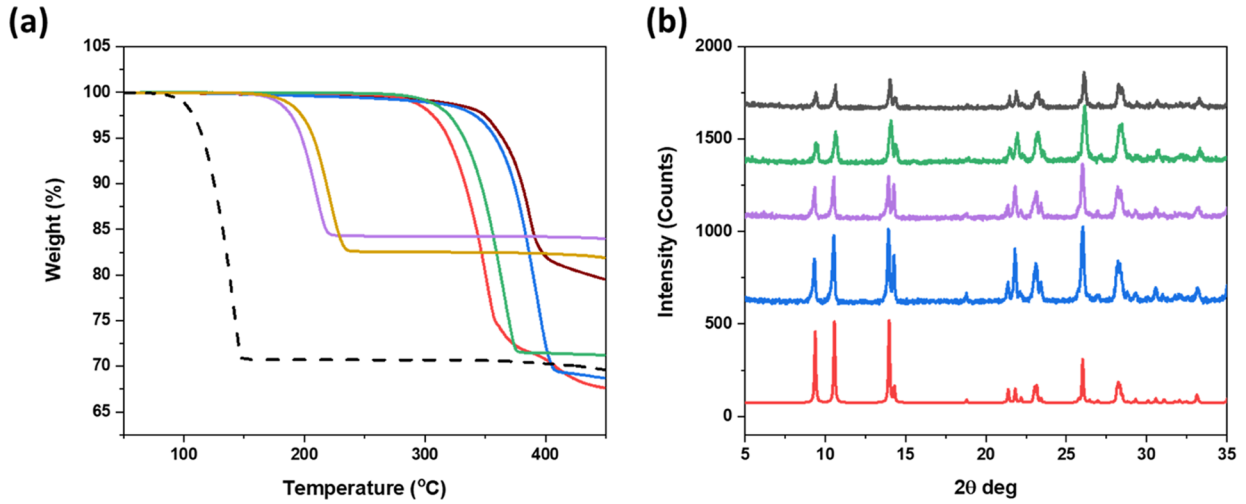


**Figure 3.** (a) TG plots of **1** (purple), **2** (yellow), **3** (green),**4** (red), **5** (blue), and **6** (brown) in comparison with that of 1D-CuI($py$) (dashed black). (b) PXRD patterns of compound **3** after various treatments. From bottom to top: simulated (red), as-made (blue), under UV light for a week (purple), soaked in water for a week (green), and heated at 180 °C for a week (black).

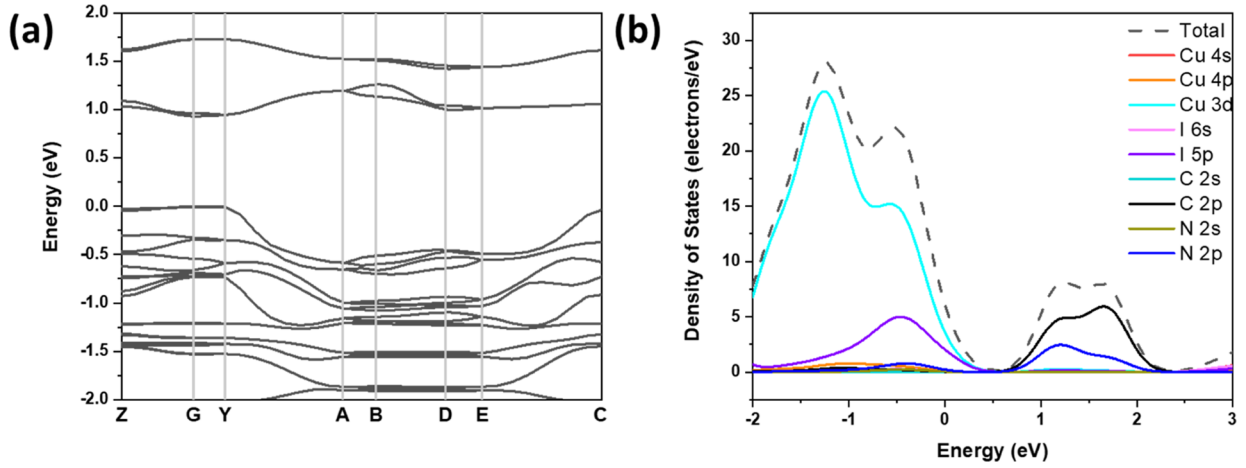


**Figure 4.** Calculated (a) band structure (BS) and (b) projected density of states (PDOS) of compound **1**. The maximum of the valence band is set at 0 eV.

only a small ac magnetic field, rms $B$ = 0.23 T, thus eliminating the need for superconducting magnets and cryogenic equipment necessary in conventional dc Hall measurements of high-mobility organic transistors.[35] An ac Hall measurement setup used in this study is shown in Figure 6a.

We drive a dc excitation current through the sample in the longitudinal direction, while an ac magnetic field of $B$ = 0.23 T (with frequency, $f$ = 0.5−2.5 Hz) is applied perpendicular to the flat facet of the crystal, and an ac Hall voltage, $V_{Hall}$, is measured by a lock-in technique in a transverse direction across the sample. To account for the contact resistance effects, a four-probe contact configuration is used, and a longitudinal four-probe voltage, $V_{4P}$, is measured along the channel as well. Hall and four-probe voltages measured in a 2D-CuI($pm$)$_{0.5}$ single crystal are shown in Figure 6b. The dc channel excitation currents, $I_{SD}$ = 0 and 40 nA, are applied intermittently, while $V_{Hall}$ and $V_{4P}$ signals are recorded. The Hall voltage, $V_{Hall}$, is found from the difference between $V_{Hall}$ (40 nA) and $V_{Hall}$ (0), which allows accounting for undesirable Faraday induction (for details, see ref 33). Hall mobility, $\mu_{Hall}$, and carrier density, $n_{Hall}$, are obtained using the following equations: $\mu_{Hall} = (D/W)\cdot V_{4P}^{-1}\cdot dV_{Hall}/dB$ and $n_{Hall} = n_{Hall} = I\cdot e^{-1}\cdot(dV_{Hall}/dB)^{-1}$, where $D$ is the distance between the voltage probes along the channel in the four-probe contact geometry


https://doi.org/10.1021/acs.chemmater.1c01421
Chem. Mater. 2021, 33, 5317−5325

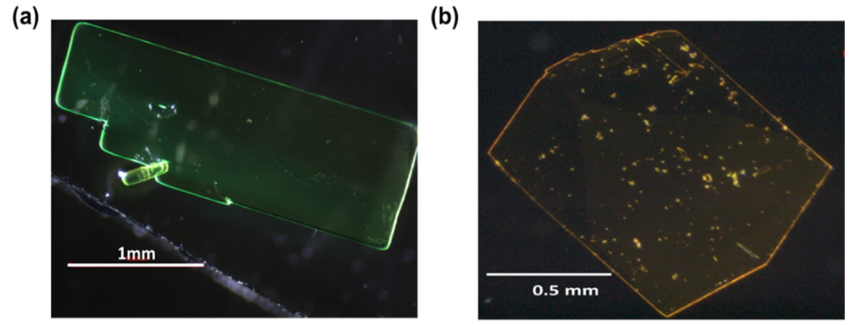


**Figure 5.** Crystal images of compounds (a) **1** and (b) **2**.

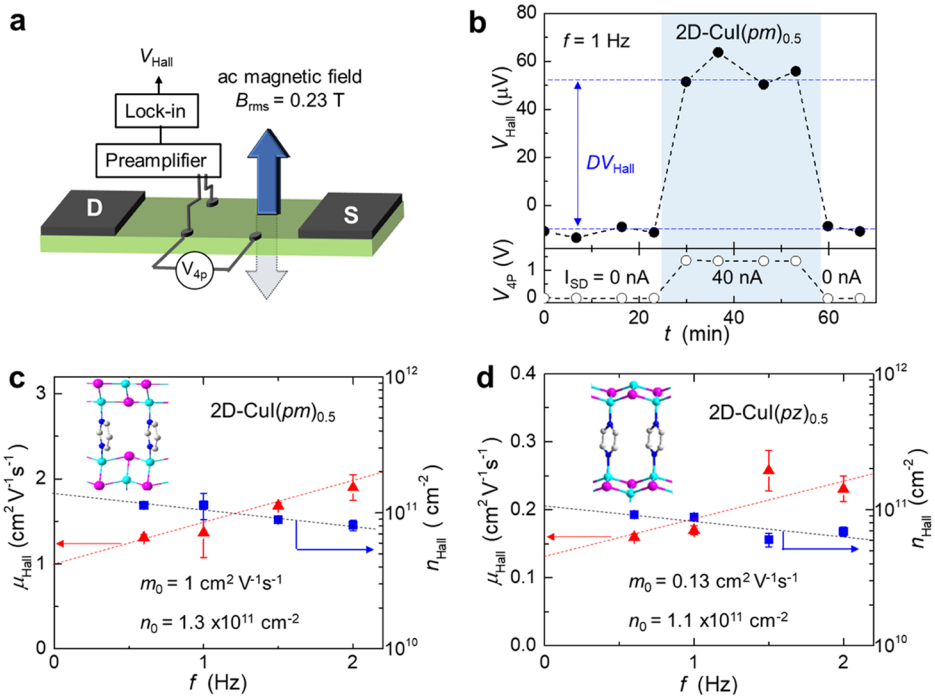


**Figure 6.** Hall-effect measurement in 2D-CuI-diazine hybrid single crystals. (a) Schematics of ac Hall-effect measurements. ac magnetic field (rms $B$ = 0.23 T) is applied perpendicular to the platelet-like crystal, while a dc excitation current is passed through the sample. dc four-probe and ac Hall voltages are monitored *in situ*. (b) Representative ac Hall voltage measured in the 2D-CuI$(pm)_{0.5}$ single crystal. The true Hall mobility, $\mu_0$, and carrier density, $n_0$, are determined by extrapolating $\mu_{Hall}(f)$ and $n_{Hall}(f)$ dependences to zero frequency ($f$ = 0) to eliminate the Faraday-induction contribution. (c) $\mu_0$ = 1 cm$^2$ V$^{-1}$ s$^{-1}$ and $n_0$ = 1.3 × 10$^{11}$ cm$^{-2}$ measured in the 2D-CuI$(pm)_{0.5}$ single crystal, and (d) $\mu_0$ = 0.13 cm$^2$ V$^{-1}$ s$^{-1}$ and $n_0$ = 1.1 × 10$^{11}$ cm$^{-2}$ measured in the 2D-CuI$(pz)_{0.5}$ single crystal.

and $W$ is the channel width. The true Hall mobility, $\mu_0$, is determined by taking these measurements at several frequencies and extrapolating $\mu_{Hall}(f)$ to zero frequency, $f$ = 0, which further helps to eliminate an unwanted Faraday induction. True carrier density, $n_0$, is also determined by extrapolation to $f$ = 0. The resultant Hall mobilities (carrier densities) are $\mu_0$ = 1 cm$^2$ V$^{-1}$ s$^{-1}$ ($n_0$ = 1.3 × 10$^{11}$ cm$^{-2}$) and 0.13 cm$^2$ V$^{-1}$ s$^{-1}$ ($n_0$ = 1.1 × 10$^{11}$ cm$^{-2}$) in 2D-CuI$(pm)_{0.5}$ and 2D-CuI$(pz)_{0.5}$ single crystals, respectively, as shown in Figure 6c,d.

The observed carrier mobilities in 2D-CuI$(pm)_{0.5}$ and 2D-CuI$(pz)_{0.5}$ single crystals are over 4 orders of magnitude higher than those in the typical strongly emissive organic semiconductors ($10^{-6}$–$10^{-5}$ cm$^2$ V$^{-1}$ s$^{-1}$).[3,4,36,37] Given the outstanding carrier mobility of these hybrids, as compared to that of known luminescent organic semiconductors, we believe that these materials are promising for the development of novel optical devices, such as light-emitting transistors.[38,39]

We also performed scanning Kelvin probe microscope (SKPM) measurements in an electrostatic force microscope mode of an atomic force microscopy (AFM) instrument (Park Systems NX-10) to determine the work function of 2D-CuI$(pm)_{0.5}$ and 2D-CuI$(pz)_{0.5}$ to make anode and cathode contacts for a single-crystal device application. SKPM provided the electrical potential mapping at room temperature in air. We extracted both work functions from the contact potential difference between the sample surface and the AFM/SKPM tip. The highly oriented pyrolytic graphite (HOPG) is used as a reference, which is stable in air with a work function of 5.5 eV obtained from ultraviolet photoelectron spectroscopy (UPS). The average potential differences of 2D-CuI$(pm)_{0.5}$ and 2D-CuI$(pz)_{0.5}$ are −34 and −240 mV, respectively, resulting in the work functions of 5.46 and 5.26 eV, respectively. 2D-CuI$(pm)_{0.5}$ displays valance band maximum (VBM)/conduction band minimum (CBM) levels of −5.4/−2.9 eV estimated from SKPM and the optical band gap. Figure 7


https://doi.org/10.1021/acs.chemmater.1c01421
Chem. Mater. 2021, 33, 5317−5325

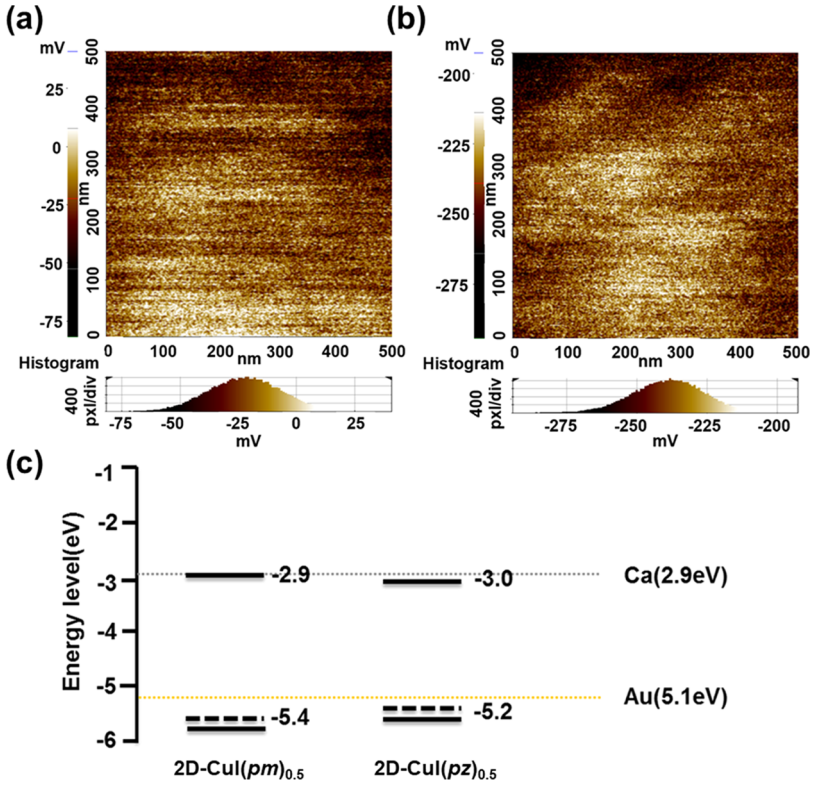


**Figure 7.** Surface potential map of (a) 2D-CuI$(pm)_{0.5}$ and (b) 2D-CuI$(pz)_{0.5}$ by SKPM in air. The relatively uniform surface potential was shown in both samples. (c) Schematic energy band diagrams of 2D-CuI$(pm)_{0.5}$ and 2D-CuI$(pz)_{0.5}$ measured by Kelvin probe microscope measurements.

shows energy levels and effective injection of electrons and holes into the hybrid crystals.

## CONCLUSIONS

A group of two-dimensional 2D-CuI$(L)_{0.5}$ structures have been synthesized and structurally characterized. These compounds exhibit systematic electronic and optical tunability similar to several other types of CuI-based hybrid semiconductor materials, including 0D-$Cu_2I_2(L)$ dimer-based and 1D-CuI$(L)$ chain-based structures.[17−19,24,40] They possess significantly improved stability as a result of increased framework dimensionality and enhanced Cu−N bonding. Their electronic structures were analyzed by DFT calculations, and their electrical and transport property measurements were carried out on high-quality, large single crystals of 2D-CuI$(pm)_{0.5}$ and 2D-CuI$(pz)_{0.5}$. The results show that both compounds display p-type conductivity in the dark, with a Hall mobility and a charge density of ~1 $cm^2\ V^{-1}\ s^{-1}$ and $1.3 \times 10^{11}\ cm^{-2}$ for 2D-CuI$(pm)_{0.5}$ and 0.13 $cm^2\ V^{-1}\ s^{-1}$ and $1.1 \times 10^{11}\ cm^{-2}$ for 2D-CuI$(pz)_{0.5}$, respectively. These values are considerably higher compared to motilities of typical highly luminescent organic semiconductors. This study demonstrates that copper iodide hybrid materials are promising for future applications in light-emitting devices.

## ASSOCIATED CONTENT

### Supporting Information

The Supporting Information is available free of charge at https://pubs.acs.org/doi/10.1021/acs.chemmater.1c01421.

Structure plots, PXRD patterns, PL spectra, and DFT calculation results (PDF)

## AUTHOR INFORMATION


### Corresponding Author

**Jing Li** − *Department of Chemistry and Chemical Biology, Rutgers University, Piscataway, New Jersey 08854, United States;* orcid.org/0000-0001-7792-4322; Email: jingli@rutgers.edu

### Authors

**Wooseok Ki** − *Department of Chemistry and Chemical Biology, Rutgers University, Piscataway, New Jersey 08854, United States; School of Natural Sciences and Mathematics, Stockton University, Galloway, New Jersey 08205, United States*

**Xiuze Hei** − *Department of Chemistry and Chemical Biology, Rutgers University, Piscataway, New Jersey 08854, United States*

**Hee Taek Yi** − *Department of Physics and Astronomy, Rutgers University, Piscataway, New Jersey 08854, United States*

**Wei Liu** − *Department of Chemistry and Chemical Biology, Rutgers University, Piscataway, New Jersey 08854, United States; Hoffman Institute of Advanced Materials, Shenzhen Polytechnic, Shenzhen 518055, China*

**Simon J. Teat** − *Advanced Light Source, Lawrence Berkeley National Laboratory, Berkeley, California 94720, United States*

**Mengjun Li** − *Department of Chemistry and Chemical Biology, Rutgers University, Piscataway, New Jersey 08854, United States*

**Yang Fang** − *Department of Chemistry and Chemical Biology, Rutgers University, Piscataway, New Jersey 08854, United States*




https://doi.org/10.1021/acs.chemmater.1c01421
Chem. Mater. 2021, 33, 5317−5325

**Vitaly Podzorov** − *Department of Physics and Astronomy, Rutgers University, Piscataway, New Jersey 08854, United States;* orcid.org/0000-0001-8276-882X

**Eric Garfunkel** − *Department of Chemistry and Chemical Biology, Rutgers University, Piscataway, New Jersey 08854, United States*

Complete contact information is available at: https://pubs.acs.org/10.1021/acs.chemmater.1c01421

### Author Contributions

#W.K. and X.H. contributed equally to this work.

### Notes

The authors declare no competing financial interest.

## ■ ACKNOWLEDGMENTS

The authors gratefully acknowledge financial support from the Materials Sciences and Engineering Division, Office of Basic Research Energy Sciences of the U.S. Department of Energy through Grant no. DE-SC0019902. The Advanced Light Source (ALS) was supported by the Director, Office of Science, Office of Basic Energy Science, of the U.S. Department of Energy, under contract DE-AC02-05CH11231. They would like to thank Dr. Hai-Lun Xia for helping with the design of an image.

## ■ REFERENCES

(1) Uoyama, H.; Goushi, K.; Shizu, K.; Nomura, H.; Adachi, C. Highly efficient organic light-emitting diodes from delayed fluorescence. *Nature* **2012**, *492*, 234−238.

(2) Zhu, X. H.; Peng, J. B.; Caoa, Y.; Roncali, J. Solution-processable single-material molecular emitters for organic light-emitting devices. *Chem. Soc. Rev.* **2011**, *40*, 3509−3524.

(3) Geens, W.; Shaheen, S. E.; Wessling, B.; Brabec, C. J.; Poortmans, J.; Serdar Sariciftci, N. Dependence of field-effect hole mobility of PPV-based polymer films on the spin-casting solvent. *Org. Electron.* **2002**, *3*, 105−110.

(4) Yersin, H.; Finkenzeller, W. J.; Walter, M. J.; Djurovich, P. I.; Thompson, M. E. *Highly Efficient OLEDs with Phosphorescent Materials*, 1st ed.; Wiley-VCH: Weinheim, Germany, 2008; p 458.

(5) Jurchescu, O. D.; Baas, J.; Palstra, T. T. M. Effect of impurities on the mobility of single crystal pentacene. *Appl. Phys. Lett.* **2004**, *84*, 3061−3063.

(6) Sundar, V. C.; Zaumseil, J.; Podzorov, V.; Menard, E.; Willett, R. L.; Someya, T.; Gershenson, M. E.; Rogers, J. A. Elastomeric Transistor Stamps: Reversible Probing of Charge Transport in Organic Crystals. *Science* **2004**, *303*, 1644−1646.

(7) Najafov, H.; Lee, B.; Zhou, Q.; Feldman, L. C.; Podzorov, V. Observation of long-range exciton diffusion in highly ordered organic semiconductors. *Nat. Mater.* **2010**, *9*, 938−943.

(8) Cai, M.; Xiao, T.; Hellerich, E.; Chen, Y.; Shinar, R.; Shinar, J. High-Efficiency Solution-Processed Small Molecule Electrophosphorescent Organic Light-Emitting Diodes. *Adv. Mater.* **2011**, *23*, 3590−3596.

(9) Zhang, X.; Sun, R.; Zheng, Q.; Kobayashi, T.; Li, W. Temperature-dependent electroluminescence from (Eu, Gd) coordination complexes. *Appl. Phys. Lett.* **1997**, *71*, 2596−2598.

(10) Baldo, M. A.; Kozlov, V. G.; Burrows, P. E.; Forrest, S. R.; Ban, V. S.; Koene, B.; Thompson, M. E. Low pressure organic vapor phase deposition of small molecular weight organic light emitting device structures. *Appl. Phys. Lett.* **1997**, *71*, 3033−3035.

(11) Tang, C. W.; VanSlyke, S. A. Organic electroluminescent diodes. *Appl. Phys. Lett.* **1987**, *51*, 913−915.

(12) Liu, W.; Zhu, K.; Teat, S. J.; Deibert, B. J.; Yuan, W.; Li, J. A mechanochemical route toward the rational, systematic, and cost-effective green synthesis of strongly luminescent copper iodide based hybrid phosphors. *J. Mater. Chem. C* **2017**, *5*, 5962−5969.

(13) Liu, W.; Zhu, K.; Teat, S. J.; Dey, G.; Shen, Z.; Wang, L.; O'Carroll, D. M.; Li, J. All-in-One: Achieving Robust, Strongly Luminescent and Highly Dispersible Hybrid Materials by Combining Ionic and Coordinate Bonds in Molecular Crystals. *J. Am. Chem. Soc.* **2017**, *139*, 9281−9290.

(14) Fang, Y.; Liu, W.; Teat, S. J.; Dey, G.; Shen, Z.; An, L.; Yu, D.; Wang, L.; O'Carroll, D. M.; Li, J. A Systematic Approach to Achieving High Performance Hybrid Lighting Phosphors with Excellent Thermal- and Photostability. *Adv. Funct. Mater.* **2017**, *27*, No. 1603444.

(15) Liu, W.; Fang, Y.; Wei, G. Z.; Teat, S. J.; Xiong, K.; Hu, Z.; Lustig, W. P.; Li, J. A Family of Highly Efficient CuI-Based Lighting Phosphors Prepared by a Systematic, Bottom-up Synthetic Approach. *J. Am. Chem. Soc.* **2015**, *137*, 9400−9408.

(16) Liu, W.; Lustig, W. P.; Li, J. Luminescent inorganic-organic hybrid semiconductor materials for energy-saving lighting applications. *EnergyChem* **2019**, *1*, No. 100008.

(17) Fang, Y.; Sojdak, C. A.; Dey, G.; Teat, S. J.; Li, M.; Cotlet, M.; Zhu, K.; Liu, W.; Wang, L.; ÓCarroll, D. M.; Li, J. Highly efficient and very robust blue-excitable yellow phosphors built on multiple-stranded one-dimensional inorganic−organic hybrid chains. *Chem. Sci.* **2019**, *10*, 5363−5372.

(18) Hei, X.; Teat, S. J.; Liu, W.; Li, J. Eco-friendly, solution-processable and efficient low-energy lighting phosphors: copper halide based hybrid semiconductors Cu4X6(L)2 (X = Br, I) composed of covalent, ionic and coordinate bonds. *J. Mater. Chem. C* **2020**, *8*, 16790−16797.

(19) Hei, X.; Liu, W.; Zhu, K.; Teat, S. J.; Jensen, S.; Li, M.; O'Carroll, D. M.; Wei, K.; Tan, K.; Cotlet, M.; Thonhauser, T.; Li, J. Blending Ionic and Coordinate Bonds in Hybrid Semiconductor Materials: A General Approach toward Robust and Solution-Processable Covalent/Coordinate Network Structures. *J. Am. Chem. Soc.* **2020**, *142*, 4242−4253.

(20) Artem'ev, A. V.; Davydova, M. P.; Hei, X.; Rakhmanova, M. I.; Samsonenko, D. G.; Bagryanskaya, I. Y.; Brylev, K. A.; Fedin, V. P.; Chen, J.-S.; Cotlet, M.; Li, J. Family of Robust and Strongly Luminescent CuI-Based Hybrid Networks Made of Ionic and Dative Bonds. *Chem. Mater.* **2020**, *32*, 10708−10718.

(21) Hei, X.; Li, J. All-in-one: a new approach toward robust and solution-processable copper halide hybrid semiconductors by integrating covalent, coordinate and ionic bonds in their structures. *Chem. Sci.* **2021**, *12*, 3805−3817.

(22) Peng, R.; Li, M.; Li, D. Copper(I) halides: A versatile family in coordination chemistry and crystal engineering. *Coord. Chem. Rev.* **2010**, *254*, 1−18.

(23) Wei, L.; Yang, F.; Jing, L. Copper Iodide Based Hybrid Phosphors for Energy-Efficient General Lighting Technologies. *Adv. Funct. Mater.* **2018**, *28*, No. 1705593.

(24) Zhang, X.; Liu, W.; Wei, G. Z.; Banerjee, D.; Hu, Z.; Li, J. Systematic Approach in Designing Rare-Earth-Free Hybrid Semiconductor Phosphors for General Lighting Applications. *J. Am. Chem. Soc.* **2014**, *136*, 14230−14236.

(25) Jeß, I.; Taborsky, P.; Pospisil, J.; Nather, C. Synthesis, crystal structure, thermal and luminescence properties of CuX(2,3-dimethylpyrazine) (X = Cl, Br, I) coordination polymers. *Dalton Trans.* **2007**, *22*, 2263−2270.

(26) Näther, C.; Greve, J.; Jeß, I. Synthesis, crystal structures and thermal properties of new copper(I) halide coordination polymers. *Solid State Sci.* **2002**, *4*, 813−820.

(27) Conesa-Egea, J.; Redondo, C. D.; Martínez, J. I.; Gómez-García, C. J.; Castillo, O.; Zamora, F.; Amo-Ochoa, P. Supramolecular Interactions Modulating Electrical Conductivity and Nanoprocessing of Copper−Iodine Double-Chain Coordination Polymers. *Inorg. Chem.* **2018**, *57*, 7568−7577.

(28) Hassanein, K.; Conesa-Egea, J.; Delgado, S.; Castillo, O.; Benmansour, S.; Martínez, J. I.; Abellán, G.; Gómez-García, C. J.; Zamora, F.; Amo-Ochoa, P. Electrical Conductivity and Strong Luminescence in Copper Iodide Double Chains with Isonicotinato Derivatives. *Chem. - Eur. J.* **2015**, *21*, 17282−17292.

(29) Blake, A. J.; Brooks, N. R.; Champness, N. R.; Cooke, P. A.; Crew, M.; Deveson, A. M.; Hanton, L. R.; Hubberstey, P.; Fenske, D.; Schröder, M. Copper(I) iodide coordination networks—controlling the placement of $(CuI)_\infty$ ladders and chains within two-dimensional sheets. *Cryst. Eng.* **1999**, *2*, 181−195.
(30) Bril, A.; De Jager-Veenis, A. W. *J. Electrochem. Soc.* **1976**, *123*, No. 396.
(31) Bai, X.; Caputo, G.; Hao, Z.; Freitas, V. T.; Zhang, J.; Longo, R. L.; Malta, O. L.; Ferreira, R. A. S.; Pinna, N. Efficient and tuneable photoluminescent boehmite hybrid nanoplates lacking metal activator centres for single-phase white LEDs. *Nat. Commun.* **2014**, *5*, No. 865.
(32) Janiak, C. A critical account on $\pi-\pi$ stacking in metal complexes with aromatic nitrogen-containing ligands. *J. Chem. Soc., Dalton Trans.* **2000**, *21*, 3885−3896.
(33) Chen, Y.; Yi, H. T.; Podzorov, V. High-Resolution ac Measurements of the Hall Effect in Organic Field-Effect Transistors. *Phys. Rev. Appl.* **2016**, *5*, No. 034008.
(34) Yi, H. T.; Gartstein, Y. N.; Podzorov, V. Charge carrier coherence and Hall effect in organic semiconductors. *Sci. Rep.* **2016**, *6*, No. 23650.
(35) Podzorov, V.; Menard, E.; Rogers, J. A.; Gershenson, M. E. Hall Effect in the Accumulation Layers on the Surface of Organic Semiconductors. *Phys. Rev. Lett.* **2005**, *95*, No. 226601.
(36) Ma, D.; Wang, G.; Hu, Y.; Zhang, Y.; Wang, L.; Jing, X.; Wang, F.; Lee, C. S.; Lee, S. T. A dinuclear aluminum 8-hydroxyquinoline complex with high electron mobility for organic light-emitting diodes. *Appl. Phys. Lett.* **2003**, *82*, 1296−1298.
(37) Assadi, A.; Svensson, C.; Willander, M.; Inganäs, O. Field-effect mobility of poly(3-hexylthiophene). *Appl. Phys. Lett.* **1988**, *53*, 195−197.
(38) Capelli, R.; Toffanin, S.; Generali, G.; Usta, H.; Facchetti, A.; Muccini, M. Organic light-emitting transistors with an efficiency that outperforms the equivalent light-emitting diodes. *Nat. Mater.* **2010**, *9*, 496−503.
(39) Zaumseil, J.; Friend, R. H.; Sirringhaus, H. Spatial control of the recombination zone in an ambipolar light-emitting organic transistor. *Nat. Mater.* **2006**, *5*, 69−74.
(40) Liu, W.; Fang, Y.; Wei, G. Z.; Teat, S. J.; Xiong, K.; Hu, Z.; Lustig, W. P.; Li, J. A Family of Highly Efficient CuI-Based Lighting Phosphors Prepared by a Systematic, Bottom-up Synthetic Approach. *J. Am. Chem. Soc.* **2015**, *137*, 9400−9408.


https://doi.org/10.1021/acs.chemmater.1c01421
*Chem. Mater.* 2021, 33, 5317−5325